Emergent Topological Phenomena in Thin Films of Pyrochlore Iridates

Bohm-Jung Yang[1] and Naoto Nagaosa[1,2]
[1]RIKEN Center for Emergent Matter Science (CEMS), Wako, Saitama 351-0198, Japan
[2]Department of Applied Physics, University of Tokyo, Tokyo 113-8656, Japan
(Received 8 January 2014; revised manuscript received 4 April 2014; published 18 June 2014)

Because of the recent development of thin film and artificial superstructure growth techniques, it is possible to control the dimensionality of the system, smoothly between two and three dimensions. In this Letter we unveil the dimensional crossover of emergent topological phenomena in correlated topological materials. In particular, by focusing on the thin film of pyrochlore iridate antiferromagnets grown along the [111] direction, we demonstrate that the thin film can have a giant anomalous Hall conductance, proportional to the thickness of the film, even though there is no Hall effect in 3D bulk material. Moreover, in the case of ultrathin films, a quantized anomalous Hall conductance can be observed, despite the fact that the system is an antiferromagnet. In addition, we uncover the emergence of a new topological phase, the nontrivial topological properties of which are hidden in the bulk insulator and manifest only in thin films. This shows that the thin film of correlated topological materials is a new platform to search for unexplored novel topological phenomena.

DOI: 10.1103/PhysRevLett.112.246402 PACS numbers: 73.43.-f, 71.70.Ej, 71.30.+h

Two quintessential ingredients governing the topological invariant of an insulator are the dimensionality and the symmetry of the system [1–4]. For instance, in two-dimensional electronic systems with broken time reversal symmetry (TRS), band insulators can be classified by the quantized Hall conductance, which generally has the form $\sigma_{xy} = (e^2/h)N$, where e is the elementary charge and h is the Planck constant [5]. Since N can be any integer, there are an infinite number of ways to distinguishing band insulators. However, when 2D and 3D electronic systems obey TRS, there are only two different ways to discern band insulators, which are based on the Z_2 topological index [6–11]. On the other hand, if 3D electronic systems break TRS, all band insulators are topologically equivalent unless additional crystalline symmetries are imposed. Considering such an intimate relationship between the topological property of band insulators and the dimensionality (and also the symmetry), one natural question is how the dimensional crossover from the 2D to 3D limit occurs in a thin film structure. In fact, it has recently been proposed that in systems with TRS, that if we make a thin film by stacking 2D topological insulators, the topological nature of the film dramatically changes depending on the parity of the number of stacked 2D layers. Such an oscillating topological property of the film eventually gives rise to a topologically nontrivial insulator in the 3D bulk limit [12].

The main purpose of this Letter is to establish a fundamental relationship between the dimensionality and the topological properties of pyrochlore iridates, $R_2Ir_2O_7$ (R = rare earth elements). In pyrochlore iridates, due to the interplay between spin-orbit coupling and electron correlation, new topological phases can appear [13,14]. For instance, a Weyl semimetal (Weyl SM), which has Fermi points [Weyl points (WP)] with a 3D Dirac-like dispersion relation around them, is proposed [15,16]. Because of the nontrivial topological properties of Weyl points, a Weyl SM has Fermi arcs on the surface, and can show an anomalous Hall effect (AHE) and a chiral magnetic effect [17,18]. Here we show that thin films of pyrochlore iridates grown along the [111] direction can show a giant AHE. In particular, in the case of ultrathin films, quantized AHE can be observed; the maximum magnitude of the anomalous Hall conductance is proportional to the thickness of the film. Moreover, we demonstrate the existence of a hidden topological phase between the Weyl SM and the fully gapped antiferromagnetic insulator (AFI) in thick films close to the bulk limit. Contrary to the common belief that Weyl SM turns directly into a trivial AFI as the strength of the local Coulomb interaction (U) increases, we show that the topological properties of the Weyl SM transfer to its neighboring gapped insulator for a finite range of U and bring about a new topological state, as summarized in Fig. 2(c).

3D bulk properties.—The pyrochlore lattice can be viewed as a face-centered cubic lattice with a tetrahedral unit cell, as shown in Fig. 1(a). In pyrochlore iridates, a Ir^{4+} ion sits on every corner of a tetrahedron. Recent theoretical and experimental studies have shown that an antiferromagnetic state with the AIAO-type local spin configuration can appear in this system for $U > U_{c1}$ [15,19–25]. In the AIAO state, four spins residing on a tetrahedron always point to, or away from, the center of the tetrahedron as shown in Fig. 1(b). The AIAO AFM supports two different types of ground states depending on U, i.e., a Weyl SM and an AFI, as described in Fig. 1(c). In fact, the Weyl SM phase has topological stability because each WP carries an integer chiral charge. Therefore a gapped insulator can be obtained

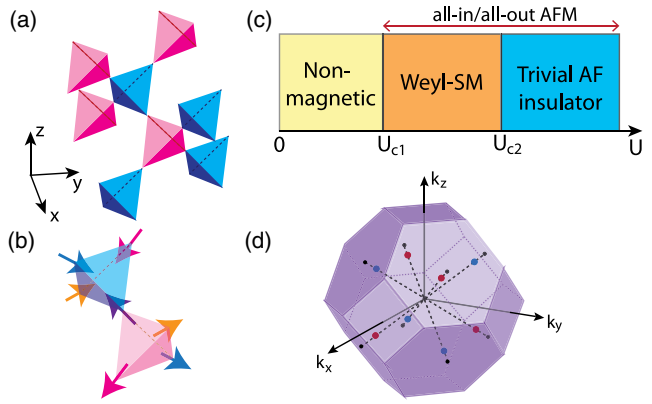

FIG. 1 (color online). (a) Structure of the pyrochlore lattice. (b) Local spin structure of the all-in–all-out (AIAO) antiferromagnet (AFM). (c) Schematic 3D bulk phase diagram as a function of local Coulomb interaction U. (d) Distribution of eight Weyl points for the Weyl SM phase. All eight WPs are aligned along the [111] or its symmetry-equivalent directions. Here a red (blue) dot indicates a WP with the chiral charge $+1$ (-1).

only when every WP is pair annihilated, by colliding with another WP with opposite chiral charge at $U = U_{c2}$.

To consistently describe the evolution of the ground state of the 3D bulk, as well as thin films, we numerically study a lattice Hamiltonian proposed in Ref. [19], i.e., $H = H_0 + (U/2)\sum_i (n_i - 1)^2$, where $H_0 = \sum_{\langle i,j\rangle} c_i^\dagger (t_1 + i t_2 \vec{d}_{ij}\cdot\vec{\sigma}) c_j + \sum_{\langle\langle i,j\rangle\rangle} c_i^\dagger (t_1' + i[t_2' \vec{R}_{ij} + t_3' \vec{D}_{ij}]\cdot\vec{\sigma}) c_j$. Here $t_{1,2}$ ($t'_{1,2,3}$) indicates the hopping amplitude between nearest-neighbor (next–nearest neighbor) sites. H_0 is a simple but realistic Hamiltonian capturing various hopping processes between the doublets, with the total angular momentum $J_{\text{eff}} = 1/2$ represented by the Pauli matrices $\sigma_{1,2,3}$. The real vectors $\vec{d}_{ij}$, $\vec{R}_{ij}$, and $\vec{D}_{ij}$ describe $\vec{\sigma}$ dependent hopping terms. Recent theoretical studies of H [19–21] have shown that when the nonmagnetic ground state is a semimetal with quadratic band crossing at the Fermi level (quadratic SM) [19,20,26,27], the Coulomb interaction U can give rise to the AIAO AFM, consistent with the first-principle calculations and experiments. Considering this, we choose the parameters of H in a way that the quadratic SM becomes the nonmagnetic ground state, and we use the AIAO AFM as a mean-field ground state. In the AIAO state, since the magnitude of the local spin moment $|\vec{m}| \equiv m$ in each site is proportional to U, we can use m as a control parameter governing the phase diagram, including the Weyl SM ($0 < m < m_{c1}$) and the gapped insulator ($m > m_{c1}$). The Weyl SM has four pairs of WPs, and each pair of WPs with opposite chiral charges is aligned along the [111] or its symmetry-equivalent directions, as shown in Fig. 1(d). Moreover, the distance between each pair increases as m increases, and finally a pair annihilation occurs at $m = m_{c1}$. It is worth noting that a recent theoretical study on a 2D bilayer of pyrochlore iridates has shown that the AIAO state can exist as the ground state even in a strictly 2D limit [28]. Therefore it is reasonable to assume the AIAO magnetic state for thin films, and to describe the dimensional crossover between 2D and 3D limits for a fixed spin configuration.

Hall conductance of Weyl SM and cubic symmetry.—In Weyl SMs, each WP behaves like a fictitious magnetic monopole producing Berry curvature [15]. Because the anomalous Hall conductivity (σ_{xy}) is proportional to the integral of the Berry curvature in the momentum space, the Weyl SM can show an intrinsic AHE. For example, for a Weyl SM with only a pair of WPs at $\pm\mathbf{k}_0 = (0, 0, \pm k_0)$, $\sigma_{xy} = (e^2/h)(2k_0/2\pi)$, where $2k_0$ is the distance between two WPs [15,29,30]. To understand the relation between the AHE and the distribution of WPs, it is convenient to introduce a Chern vector $\vec{C} = (C_x, C_y, C_z)$, which is defined as $\sigma_{ij} = (e^2/2\pi h)\epsilon_{ijk} C_k$, where ϵ_{ijk} is the fully antisymmetric tensor with $\epsilon_{123} = 1$ [29,31]. Therefore, for a pair of WPs located at $\pm\mathbf{k}_0 = (0, 0, \pm k_0)$, the corresponding Chern vector is $\vec{C} = (0, 0, 2k_0)$. In the case of the Weyl SM in pyrochlore iridates, there are four pairs of WPs, due to the cubic symmetry. Since a Chern vector $\vec{C}$ can be assigned to each pair of WPs, there are in total four Chern vectors $\vec{C}_{1,2,3,4}$ with $\pm\frac{1}{2}\vec{C}_{1,2,3,4}$ corresponding to the location of the WPs. However, since all WPs are related by the cubic symmetry, $\sum_{i=1}^{4} \vec{C}_i = 0$. Therefore the total Hall current should be zero in the 3D bulk. However, it should be stressed that although the net Chern vector is zero, the Weyl SM is still topologically nontrivial because there exist finite Chern vectors that are antiferromagnetically aligned. Once the cubic symmetry is broken, the incomplete cancellation of Chern vectors can generate nontrivial responses, which is the fundamental origin of emergent topological phenomena in thin films.

Topological properties of [111] thin films.—Viewed along the [111] direction ("z direction" hereafter), the pyrochlore lattice is made of vertically stacked bilayers, composed of neighboring kagome and triangular layers [Fig. 2(a)]. Because of such a peculiar lattice structure, the [111] plane provides a natural direction for film growth. In the following, we examine how the topological properties of thin films evolve as the number of bilayers (N_b) increases, by computing the Hall conductance G_{xy} numerically. Since the finite thickness of the film induces a small gap at WPs, bulk states in general do not touch the Fermi level for any $m > 0$; hence, G_{xy} is expected to be quantized. However, the nontrivial topological property of the bulk states supports surface states (SSs) in the gap, which disturb the quantization of G_{xy} in films. To understand the interplay between the bulk and surface states, we also compute the maximum Hall conductance $G_{xy}^{\max}$ by imposing the half-filling condition at each momentum $\mathbf{k}$ locally and adding the Berry curvature of locally half-filled bands over the entire Brillouin zone (BZ). Because the Fermi level can be in the gap locally in each $\mathbf{k}$ in this case, $G_{xy}^{\max}$ can be quantized.

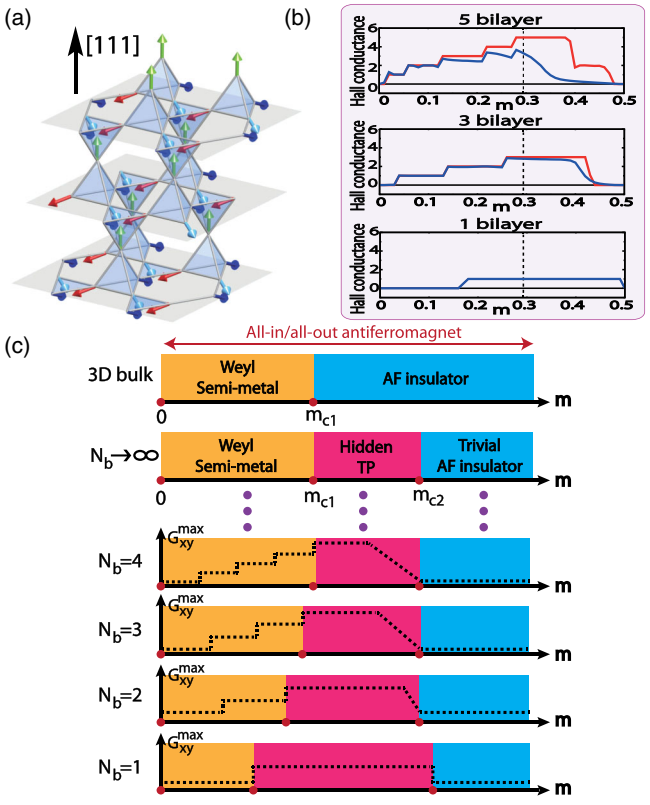

FIG. 2 (color online). (a) Lattice structure of [111] thin films. (b) The detailed changes of G_{xy} (blue) and $G_{xy}^{\max}$ (red). For $N_b = 1$, G_{xy} and $G_{xy}^{\max}$ are the same. The vertical dotted line indicates the critical point m_{c1}. (c) Evolution of the phase diagram of [111] thin films as the number of bilayers N_b increases. The top (bottom) surface of each film is terminated by a triangular (kagome) layer. The dotted lines schematically describe the change of maximum anomalous Hall conductance $G_{xy}^{\max}$ of the system.

As shown in Fig. 2(c), the phase diagram of thin films has unexpected rich structures. At first, when $0 < m < m_{c1}$, $G_{xy}^{\max} = L_z\sigma_{xy}$ ($L_z = N_b a_z$ is the length of the film) increases monotonically as m increases, and eventually reaches the maximum value of $G_{xy}^{\max} = (e^2/h)N_b$ near $m = m_{c1}$. To understand this, let us note that the change of $G_{xy}^{\max}$ describes a topological phase transition induced by an accidental gap closing. In fact, a gapless WP of the bulk Weyl SM turns into a group of 2D gapped Dirac points (GDPs) in films, because k_z becomes discrete due to the finite size effect. By changing m, whenever an accidental gap closing occurs at a GDP, $G_{xy}^{\max}$ shows a discontinuous change of $\Delta G_{xy}^{\max} = \pm(e^2/h)$ [32]. Therefore, to understand the nontrivial variation of $G_{xy}^{\max}$, it is necessary to figure out the gap-closing condition at a GDP under the open boundary condition (BC) relevant to thin films. After straightforward calculations, one can show that the energy of the conduction band minimum (E_c) and the valence band maximum (E_v) of a GDP is $E_{c/v} = \pm\varepsilon(n) + \alpha$, where $\varepsilon(n) = v(n + 1/2)\pi/L_z$ ($n = 0, 1, 2, \ldots$) with the velocity v, and α is a constant. (See Supplemental Material [33].) Since the variation of the parameter α merely induces an overall shift of the energy spectrum near each GDP, the gap is fixed irrespective of α. Hence a gap closing cannot be achieved at a single GDP by varying α. However, when a pair of WPs are coupled due to the open BC, the energy spectra for GDPs show completely different behavior. For such a pair of WPs, $E_{c,v}$ are $E_{c1/v1} = \pm\varepsilon'(n) + \alpha + \beta$ and $E_{c2/v2} = \pm\varepsilon'(n) - \alpha + \beta$, respectively. Here $\varepsilon'(n) = 2n\pi/L_z$ and α, β are constants. Note that although the gap of each GDP is fixed, the relative energy between two GDPs (for example, $E_{c1} - E_{v2}$) depends on a parameter α; hence, a gap closing is possible by tuning α. It is worth noting that in [111] films, there is always a pair of WPs aligned along the z direction. Under the open BC, these two WPs are coupled and projected to the center of the surface BZ, while the other six WPs are projected to six other independent momentum points. Therefore successive gap closing is possible only at the Γ point leading to monotonic stepwise increment of $G_{xy}^{\max}$. Since the largest Hall conductance achievable through a pair of WPs is equal to $(e^2/h)N_b$, this limits the upper bound for $G_{xy}^{\max}$. Contrary to $G_{xy}^{\max}$, the quantized G_{xy} can be observed only in ultrathin films with $N_b < 4$ due to SS, as shown in Fig. 2(b). However, the overall change of G_{xy} follows $G_{xy}^{\max}$, and giant G_{xy} can be observed near $m = m_{c1}$.

The hidden topological phase.—Another intriguing aspect of Fig. 2(c) is that a finite AHE can be observed even beyond the bulk quantum critical point (m_{c1}). Since bulk states are fully gapped for $m > m_{c1}$, the variation of $G_{xy}^{\max}$ is possible only if the film supports intrinsic SSs connecting the bulk valence and conduction bands. To understand such a nontrivial variation of $G_{xy}^{\max}$, let us first describe the surface spectrum of a thick film, which has kagome lattice on both the top and bottom surfaces. As shown in Fig. 3(a), when $0 < m < m_{c1}$, there are three pairs of Fermi arcs in the surface BZ whose end points correspond to the projection of bulk WPs to the surface. As m increases, the size of the Fermi arcs increases until they hit the BZ boundary at $m = m_{c1}$, signaling a Lifshitz

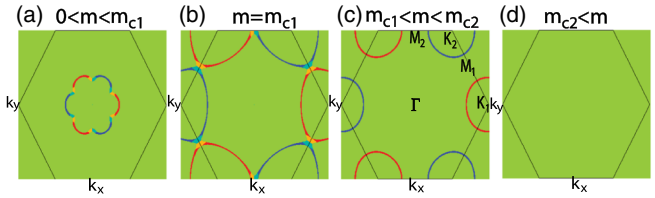

FIG. 3 (color online). Fermi surface shape due to localized in-gap states. Here the film is composed of 20 bilayers with an additional kagome layer on the top; hence, it has kagome layers on both the top and bottom surfaces. The red (blue) lines indicate the states at E_F localized on the top (bottom) surfaces, and there is no surface state in the green region. For $0 < m < m_{c2}$, the surface states maintain the chiral nature, suppressing backscatterings.

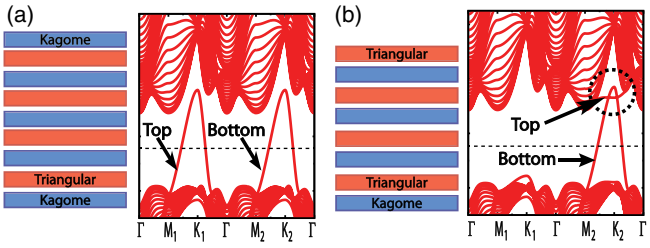

FIG. 4 (color online). (a) A film terminated by kagome layers on both the top and bottom surfaces when $m_{c1} < m < m_{c2}$. Two bands touching the Fermi level (the dotted horizontal line) are SSs, localized on the top (left band) and bottom (right band) kagome layers, respectively. (b) A film terminated by a triangular (kagome) layer on the top (bottom) surface. Both top and bottom surfaces support SSs, which are crossing in the gap (marked by a dotted circle).

transition [Fig. 3(b)]. When $m > m_{c1}$, the Fermi surface turns into two different closed loops centered at the corners of the BZ, respectively [Fig. 3(c)]. It is worth noting that the surface spectrum persists in the gap even when $m > m_{c1}$, which eventually disappears when $m > m_{c2}$ [Fig. 3(d)].

On the other hand, when the unit bilayers are stacked along the z direction, the top and bottom surfaces have different lattice structures [Fig. 4(b)]. One interesting property of the surface terminated by a triangular lattice is that there are additional localized SSs, which are not of topological origin [33]. In fact, because of the lattice geometry, many localized states that are confined around each hexagonal plaquette of the lattice can appear in the pyrochlore lattice [36]. Such lattice geometry–induced localized states can induce remarkable physical consequences, such as the emergence of a flat band with a large Chern number when a suitable spin-orbit coupling is added to the Hamiltonian [37]. In pyrochlore iridate thin films, the geometry-induced SS induces the coupling between the valence and conduction bands when $m > m_{c1}$, as shown in Fig. 4(b). Here, the two in-gap states crossing near the momentum K_2 are SSs localized on the top and bottom surfaces, respectively. By comparing Figs. 4(a) and 4(b), one can see that the SS smoothly connected to the valence band is nothing but the SS of topological origin related with the Weyl SM, whereas the other SS connected to the conduction band is a lattice geometry–induced SS. Such a crossing between two SSs induces a huge change in G_{xy} and $G_{xy}^{\max}$, finally leading to the trivial AFI at $m = m_{c2}$, beyond which two SSs decouple and $G_{xy}^{\max}$ vanishes.

Discussion.—As described above, thin films of pyrochlore iridates offer a unique opportunity, which has various aspects. (i) This is the first realistic AFM showing the quantized AHE due to the scalar spin chirality without the uniform magnetization [38]. The antiferromagnetic phase has two degenerate ground states, i.e., the AIAO state and its time-reversed partner. Because the Hall conductances of these two phases have the opposite sign, metallic conducting channels can appear at domain walls. (ii) The bulk-surface correspondence of the hidden topological phase belongs to a new class; i.e., the SSs carry large Chern numbers, which in principle can be proportional to the thickness $L_z = N_b a_z$ of the film, while the 3D bulk system ($L_z \to \infty$) is not topological, with zero Chern number. This apparently contradictory behavior is explained by the fact that exponentially small overlap, i.e., $\sim \exp(-L_z/\xi)$ ($\xi \sim ta/E_G$ is the correlation length determined by the transfer integral t, the band gap E_G, and the lattice constant a), between the SSs on the top and bottom produces the Chern numbers; hence, this carries the information about the bulk. In the limit of $L_z \to \infty$, this overlap can be neglected and the Chern number vanishes.

Recent experiments on $Nd_2(Ir_{1-x}Rh_x)_2O_7$ have shown that conducting channels localized at domain walls exist in both the insulating and semimetallic samples [39,40]. Our study clearly shows that the SSs associated with the antiferromagnetically aligned Chern vectors can appear in both the insulating and Weyl semimetallic phases, consistent with the experiment. Although the domain wall is different from the open surface of films in a strict sense, the emerging metallic states share the same topological origin [41].

We conclude with a discussion about fluctuation effects. There is a lot of experimental evidence supporting the AIAO state in $R_2Ir_2O_7$ (R = Nd, Eu, Y) [23–25]. These materials have the insulating ground state because the local moment m is large enough to induce the pair annihilation of WPs. Hence, in bulk materials, the Weyl SM can be observed only near the vicinity of the metal-insulator transition temperature where m is small. However, in thin films, due to the enhanced fluctuation effects induced by the finite thickness, m can be reduced significantly. (See Supplemental Material [33].) Therefore fabricating thin films is a promising way to observe the exotic properties of the Weyl SM in pyrochlore iridates.

We greatly appreciate the stimulating discussions with David Vanderbilt. We are grateful for support from the Japan Society for the Promotion of Science (JSPS) through the Funding Program for World-Leading Innovative R&D on Science and Technology (FIRST Program).

[1] A. P. Schnyder, S. Ryu, A. Furusaki, and A. W. W. Ludwig, Phys. Rev. B **78**, 195125 (2008).
[2] A. P. Schnyder, S. Ryu, A. Furusaki, and A. W. W. Ludwig, AIP Conf. Proc. **1134**, 10 (2009).
[3] A. Kitaev, AIP Conf. Proc. **1134**, 22 (2009).
[4] X.-L. Qi, T. L. Hughes, and S.-C. Zhang, Phys. Rev. B **78**, 195424 (2008).
[5] F. D. M. Haldane, Phys. Rev. Lett. **61**, 2015 (1988).
[6] C. L. Kane and E. J. Mele, Phys. Rev. Lett. **95**, 146802 (2005).

[7] C. L. Kane and E. J. Mele, Phys. Rev. Lett. **95**, 226801 (2005).
[8] L. Fu, C. L. Kane, and E. J. Mele, Phys. Rev. Lett. **98**, 106803 (2007).
[9] J. E. Moore and L. Balents, Phys. Rev. B **75**, 121306 (2007).
[10] R. Roy, Phys. Rev. B **79**, 195322 (2009).
[11] A. M. Essin, J. E. Moore, and D. Vanderbilt, Phys. Rev. Lett. **102**, 146805 (2009).
[12] C.-X. Liu, H. J. Zhang, B. Yan, X.-L. Qi, T. Frauenheim, X. Dai, Z. Fang, and S.-C. Zhang, Phys. Rev. B **81**, 041307(R) (2010).
[13] B. J. Kim, H. Jin, S. J. Moon, J.-Y. Kim, B.-G. Park, C. S. Leem, J. Yu, T. W. Noh, C. Kim, S.-J. Oh, J.-H. Park, V. Durairaj, G. Cao, and E. Rotenberg, Phys. Rev. Lett. **101**, 076402 (2008).
[14] B. J. Kim, H. Ohsumi, T. Komesu, S. Sakai, T. Morita, H. Takagi, and T. Arima, Science **323**, 1329 (2009).
[15] X. Wan, A. M. Turner, A. Vishwanath, and S. Y. Savrasov, Phys. Rev. B **83**, 205101 (2011).
[16] W. Witczak-Krempa, G. Chen, Y. B. Kim, and L. Balents, Annu. Rev. Condens. Matter Phys. **5**, 57 (2014).
[17] A. A. Zyuzin and A. A. Burkov, Phys. Rev. B **86**, 115133 (2012).
[18] P. Goswami and S. Tewari, Phys. Rev. B **88**, 245107 (2013).
[19] W. Witczak-Krempa, A. Go, and Y. B. Kim, Phys. Rev. B **87**, 155101 (2013).
[20] W. Witczak-Krempa and Y. B. Kim, Phys. Rev. B **85**, 045124 (2012).
[21] A. Go, W. Witczak-Krempa, G. S. Jeon, K. Park, and Y. B. Kim, Phys. Rev. Lett. **109**, 066401 (2012).
[22] T. Arima, J. Phys. Soc. Jpn. **82**, 013705 (2013).
[23] H. Sagayama, D. Uematsu, T. Arima, K. Sugimoto, J. J. Ishikawa, E. O'Farrell, and S. Nakatsuji, Phys. Rev. B **87**, 100403(R) (2013).
[24] K. Tomiyasu, K. Matsuhira, K. Iwasa, M. Watahiki, S. Takagi, M. Wakeshima, Y. Hinatsu, M. Yokoyama, K. Ohoyama, and K. Yamada, J. Phys. Soc. Jpn. **81**, 034709 (2012).
[25] S. M. Disseler, arXiv:1403.6389.
[26] B.-J. Yang and Y. B. Kim, Phys. Rev. B **82**, 085111 (2010).
[27] E.-G. Moon, C. Xu, Y. B. Kim, and L. Balents, Phys. Rev. Lett. **111**, 206401 (2013).
[28] X. Hu, A. Ruegg, and G. A. Fiete, Phys. Rev. B **86**, 235141 (2012).
[29] K.-Y. Yang, Y.-M. Lu, and Y. Ran, Phys. Rev. B **84**, 075129 (2011).
[30] A. A. Burkov and L. Balents, Phys. Rev. Lett. **107**, 127205 (2011).
[31] B. I. Halperin, Jpn. J. Appl. Phys., Suppl. **26**, 1913 (1987).
[32] M. Oshikawa, Phys. Rev. B **50**, 17357 (1994).
[33] See Supplemental Material at http://link.aps.org/supplemental/10.1103/PhysRevLett.112.246402 for further details of the calculation, which includes Refs. [34, 35].
[34] E. McCann and V. I. Fal'ko, J. Phys. Condens. Matter **16**, 2371 (2004).
[35] A. R. Akhmerov and C. W. J. Beenakker, Phys. Rev. B **77**, 085423 (2008).
[36] D. L. Bergman, C. Wu, and L. Balents, Phys. Rev. B **78**, 125104 (2008).
[37] M. Trescher and E. J. Bergholtz, Phys. Rev. B **86**, 241111 (R) (2012).
[38] R. Shindou and N. Nagaosa, Phys. Rev. Lett. **87**, 116801 (2001); I. Martin and C. D. Batista, Phys. Rev. Lett. **101**, 156402 (2008).
[39] K. Ueda, J. Fujioka, Y. Takahashi, T. Suzuki, S. Ishiwata, Y. Taguchi, and Y. Tokura, Phys. Rev. Lett. **109**, 136402 (2012).
[40] K. Ueda, J. Fujioka, Y. Takahashi, T. Suzuki, S. Ishiwata, Y. Taguchi, M. Kawasaki, and Y. Tokura, Phys. Rev. B **89**, 075127 (2014).
[41] Y. Yamaji and M. Imada, arXiv:1306.2022.